

Article

One-Step Sintering Process for the Production of Magnetocaloric La(Fe,Si)₁₃-Based Composites

Xi-Chun Zhong ^{1,*} , Xu-Tao Dong ¹, Jiao-Hong Huang ², Cui-Lan Liu ², Hu Zhang ³, You-Lin Huang ⁴, Hong-Ya Yu ¹ and Raju V. Ramanujan ^{5,6}

¹ School of Materials Science and Engineering, South China University of Technology, Guangzhou 510640, China; xutaodonga@gmail.com (X.-T.D.); yuhongya@scut.edu.cn (H.-Y.Y.)

² Baotou Research Institute of Rare Earths, Baotou 014030, China; jiaohongh@163.com (J.-H.H.); liucuilan618@126.com (C.-L.L.)

³ School of Materials Science and Engineering, University of Science and Technology Beijing, Beijing 100083, China; zhanghu@ustb.edu.cn

⁴ School of Materials Science and Engineering, Nanchang Hangkong University, Nanchang 330063, China; hyl1019_lin@163.com

⁵ School of Materials Science and Engineering, Nanyang Technological University, Singapore 639798, Singapore; ramanujan@ntu.edu.sg

⁶ Singapore-HUJ Alliance for Research and Enterprise (SHARE), Nanomaterials for Energy and Energy-Water Nexus (NEW), Campus for Research Excellence and Technological Enterprise (CREATE), Singapore 138602, Singapore

* Correspondence: xczhong@scut.edu.cn



Citation: Zhong, X.-C.; Dong, X.-T.; Huang, J.-H.; Liu, C.-L.; Zhang, H.; Huang, Y.-L.; Yu, H.-Y.; Ramanujan, R.V. One-Step Sintering Process for the Production of Magnetocaloric La(Fe,Si)₁₃-Based Composites. *Metals* **2022**, *12*, 112. <https://doi.org/10.3390/met12010112>

Academic Editors: Volodymyr A. Chernenko and Daniel Fruchart

Received: 9 November 2021

Accepted: 4 January 2022

Published: 6 January 2022

Publisher's Note: MDPI stays neutral with regard to jurisdictional claims in published maps and institutional affiliations.



Copyright: © 2022 by the authors. Licensee MDPI, Basel, Switzerland. This article is an open access article distributed under the terms and conditions of the Creative Commons Attribution (CC BY) license (<https://creativecommons.org/licenses/by/4.0/>).

Abstract: A one-step sintering process was developed to produce magnetocaloric La(Fe,Si)₁₃/Ce-Co composites. The effects of Ce₂Co₇ content and sintering time on the relevant phase transformations were determined. Following sintering at 1373 K/30 MPa for 1–6 h, the NaZn₁₃-type (La,Ce)(Fe,Co,Si)₁₃ phase formed, the mass fraction of α -Fe phase reduced and the CeFe₇-type (La,Ce)(Fe,Co,Si)₇ phase appeared. The mass fraction of the (La,Ce)(Fe,Co,Si)₇ phase increased, and the α -Fe phase content decreased with increasing Ce₂Co₇ content. However, the mass fraction of the (La,Ce)(Fe,Co,Si)₇ phase reduced with increasing sintering time. The EDS results showed a difference in concentration between Co and Ce at the interphase boundary between the 1:13 phase and the 1:7 phase, indicating that the diffusion mode of Ce is reaction diffusion, while that of Co is the usual vacancy mechanism. Interestingly, almost 100% single phase (La,Ce)(Fe,Co,Si)₁₃ was obtained by appropriate Ce₂Co₇ addition. After 6 h sintering at 1373 K, the Ce and Co content in the (La,Ce)(Fe,Co,Si)₁₃ phase increased for larger Ce₂Co₇ content. Therefore, the Curie temperature increased from 212 K (binder-free sample) to 331 K (15 wt.% Ce₂Co₇ sample). The maximum magnetic entropy change ($-\Delta S_M$)^{max} decreased from 8.8 (binder-free sample) to 6.0 J/kg·K (15 wt.% Ce₂Co₇ sample) under 5 T field. High values of compressive strength (σ_{bc})^{max} of up to 450 MPa and high thermal conductivity (λ) of up to 7.5 W/m·K were obtained. A feasible route to produce high quality La(Fe,Si)₁₃ based magnetocaloric composites with large MCE, good mechanical properties, attractive thermal conductivity and tunable T_C by a one-step sintering process has been demonstrated.

Keywords: La(Fe,Si)₁₃ based composites; sintering; grain boundary diffusion; magnetocaloric effect

1. Introduction

Climate change is of high global significance, resulting in high interest in more efficient cooling systems. Therefore, there is considerable research interest in the emerging attractive topic of magnetic refrigeration (MR) [1,2]. Advances in magnetocaloric materials (MCMs) are urgently needed to realize the promise of MR. MCMs which exhibit a giant magnetocaloric effect (MCE) include Gd₅(Si_xGe_{1-x})₄ [3,4], MnFe(P,As) [5], Mn(Fe,Co)Ge [6], LaFe_{13-x}Si_x [7,8], and Heusler alloys [9], which undergo a first-order magnetic transition (FOMT) near their Curie temperatures (T_{CS}). Recently, other materials,

such as $\text{RE}_2\text{ZnMnO}_6$ (RE = Gd, Dy, and Ho) perovskites [10], $\text{RE}_2\text{FeAlO}_6$ (RE = Gd, Dy, Ho) oxides [11], $\text{RE}_{60}\text{Co}_{20}\text{Ni}_{20}$ (RE = Ho and Er) amorphous ribbons [12], $\text{LaFe}_{12}\text{B}_6$ -based materials [13], and rare earth-based intermetallic compounds [14], were found to exhibit outstanding magnetocaloric performance at cryogenic temperatures. The development of these materials can promote the development of magnetic refrigeration technology.

NaZn_{13} -type $\text{La}(\text{Fe},\text{Si})_{13}$ compounds have attracted considerable attention as magnetocaloric materials due to their large magnetocaloric effect (MCE) values, relatively low cost, tunable Curie temperature (T_C), and environmental friendliness [1,7,15]. However, these compounds have some disadvantages [16–18]: First, it is difficult to form single-phase $\text{La}(\text{Fe},\text{Si})_{13}$ material. An ingot of $\text{La}(\text{Fe},\text{Si})_{13}$ has to be annealed above 1273 K for several days or even a month to obtain a single phase [18]. Second, the T_C of $\text{LaFe}_{13-x}\text{Si}_x$ ($1.0 \leq x \leq 1.6$) compounds is less than 210 K, which is too low for near room temperature magnetic cooling. Third, these compounds show a first-order magnetic transition (FOMT), which has a desirable large magnetic entropy change, but is accompanied by thermal and magnetic hysteresis and relatively large undesirable changes in crystal symmetry and/or volume [17]. The magneto-volume effect can lead to pulverization of bulk $\text{LaFe}_{13-x}\text{Si}_x$ magnetocaloric materials when the magnetic field is varied during the MR process [17]. The brittleness and magnetic volume change reduce formability, limiting the progress of this material for commercial applications.

Considerable research has been performed to overcome these shortcomings. Short time annealing produced a single phase material in melt-spun samples [19]. Combining kilogram-scale strip-casting with short time annealing has been deployed for mass production of $\text{LaFe}_{13-x}\text{Si}_x$ -based magnetic cooling materials [20]. Elemental substitution of Fe (by Co [18,21,22], Si [23], etc.) or La (by Ce [24]) can improve magnetocaloric performance. T_C can be raised from ~200 K to room temperature or even higher by addition of interstitial atoms like H [23,25–27]. Hydrogenation of $\text{LaFe}_{13-x}\text{Si}_x$ is the most effective method to shift T_C to room temperature while maintaining a large magnetocaloric effect [28]. Quaternary $\text{La}(\text{Fe},\text{Co},\text{Si})_{13}$ compounds can increase T_C and change the magnetic transition from first-order to second-order, accompanied by lower MCE.

$\text{LaFe}_{13-x}\text{Si}_x$ bulk composites can be prepared through powder metallurgy technology using $\text{LaFe}_{13-x}\text{Si}_x$ particles and binder powder as raw materials. Although $\text{LaFe}_{13-x}\text{Si}_x$ is hard and brittle, particle fracture can be avoided by adding low hardness binders during the powder metallurgy process. Additionally, the magneto-volume effect can be reduced by pulverization of the material [29]. Various binder materials, such as polymers [30], high thermal conductivity metals [31], and low melting alloys [32,33], have been studied to obtain high performance using relatively low sintering temperatures. High-temperature sintering will lead to metallurgical reactions between the binder and the particles, it will also significantly decrease the mass fraction of the 1:13 phase and lower the MCE of the composites [31]. The magnetocaloric properties of the composites arise from the La-Fe-Si based alloy. Addition of binder material reduces the mass fraction of magnetocaloric material and decreases the MCE of the composites.

La-Co alloys [34,35] have been used as binder due to the low enthalpy of formation of the LaCo_{13} phase (−5.79 kJ/mol) [36], lower La-Fe binary phase content and the low melting point of a La-based eutectic alloy [37]. Based on grain boundary diffusion (GBD) theory [38], Co diffusion occurs through annealing after hot pressing [34,39]. During annealing, Co can diffuse into the 1:13 matrix, influencing the magnetic and magnetocaloric properties and promoting the formation of the 1:13 phase. The binder content and annealing parameters play an important role in the phase formation process. For example, addition of more than 5 wt.% of La-Al alloy was detrimental to 1:13 phase formation in La-Fe-Si/La-Al composites [40]. Our previous work [41] showed that excess addition of Ce-Co alloy binder would result in the formation of a new phase, which disappeared with increasing heat treatment time. However, the sintering temperature is below the melting point of $\text{Ce}_{40}\text{Co}_{60}$ (1323 K), resulting in a porous structure and insufficient mechanical properties. The large pressure of hot pressing (600 MPa) and long diffusion annealing times (up to 24 h) are

unfavorable for industrial production. To overcome these limitations, we combined the advantages of hot pressing and diffusion annealing in this work. We developed a novel process to prepare La-Fe-Si-based composites by sintering to shorten the processing time and improve the compressive properties. The effect of Ce_2Co_7 binder on the formation of the 1:13 phase, thermal conductivity, mechanical, magnetic and magnetocaloric properties of $\text{LaFe}_{11.6}\text{Si}_{1.4}/\text{Ce}_2\text{Co}_7$ composites was studied. The diffusion mechanism of Ce and Co was also investigated. The T_C increased from ~ 200 K to near room temperature. High values of the compressive strength $(\sigma_{bc})^{\text{max}}$ of up to 450 MPa and of the thermal conductivity (λ) of up to 7.5 W/m·K were successfully obtained.

2. Experimental Section

Annealed $\text{LaFe}_{11.6}\text{Si}_{1.4}$ flakes were prepared following the procedure described in our previous work [41]. The Ce_2Co_7 compounds were prepared by an arc melting process with pure Ce (≥ 99.5 wt.%) and Co (≥ 99.9 wt.%). The annealed $\text{LaFe}_{11.6}\text{Si}_{1.4}$ flakes were mechanically milled to powders with a particle size in the range of 45 to 100 μm . Ce_2Co_7 fine powders were prepared with a particle size smaller than 30 μm . The $\text{LaFe}_{11.6}\text{Si}_{1.4}$ and Ce_2Co_7 powders were homogeneously mixed with 0, 5, 10, and 15 wt.% content of Ce_2Co_7 powder, followed by sintering under uniaxial stress of 30 MPa at 1373 K to produce cylindrical samples with 15 mm in diameter and 5 mm in height.

XRD characterization was carried out using X-ray diffractometer (Rigaku D/max-2200/PC, Tokyo, Japan) with $\text{Cu-K}\alpha_1$ radiation ($\lambda = 1.54056 \text{ \AA}$) at a scan rate of $2^\circ/\text{min}$. The phase compositions and microstructures were analyzed by a thermal field emission scanning electron microscope (SEM, FEI Nova Nano SEM 430, Davis, CA, USA) equipped with an energy-dispersive spectrometer (EDS) attachment. Measurements of thermal conductivity and magnetic properties were carried out using a Physical Property Measurement System (PPMS-9, Quantum Design, San Diego, CA, USA). The compressive strengths of the samples were measured by a mechanical testing system (Shimadzu AG-100NX, Kyoto, Japan). The porosity (P) of the composites were determined by the following equation: $P = 1 - \rho/\rho_0$, where ρ is the effective density and ρ_0 is the theoretical density. The effective density (ρ) of each sample was tested by the Archimedes method. The theoretical density (ρ_0) of each sample was calculated by the following equation: $\rho_0 = \frac{100}{\sum_i \frac{m_i}{\rho_i}}$, where m_i was the mass of the corresponding phase in the 100 g sample and the ρ_i was the density of the specific phase.

3. Results and Discussion

3.1. Phase Analysis

Figure 1a shows the Rietveld refined X-ray diffraction (XRD) patterns of $\text{LaFe}_{11.6}\text{Si}_{1.4}/x$ wt.% Ce_2Co_7 ($x = 0, 5, 10,$ and 15) composites sintered at 1373 K for 6 h. $\text{LaFe}_{11.6}\text{Si}_{1.4}/x$ wt.% Ce_2Co_7 ($x = 5, 10,$ and 15) sintered composites exhibited a majority 1:13 phase. The α -Fe phase content decreased, corresponding to the appearance of a CeFe_7 -type phase (1:7 phase) and a La_2O_3 phase. For composites sintered at 1373 K for 6 h, higher Ce_2Co_7 binder content (less than 15 wt.%) can promote formation of the 1:13 phase and decrease the α -Fe phase content (Figure 1a and Table 1).

For example, $\text{LaFe}_{11.6}\text{Si}_{1.4}/5\text{wt.}\%\text{Ce}_2\text{Co}_7$ composites contained 93.21 wt.% 1:13 phase, 5.90 wt.% α -Fe phase and a small amount of 1:7 phase (0.89 wt.%). However, when the addition of Ce_2Co_7 binder rose to 10 wt.% or more, the mass fraction of 1:7 phase increased. Moreover, the mass fraction of 1:7 phase in the $\text{LaFe}_{11.6}\text{Si}_{1.4}/10$ wt.% Ce_2Co_7 composites decreased with an increase in sintering time. As reported earlier [41], the 1:7 phase occurred at grain boundaries after annealing for a short time. Clearly, the 1:7 phase content after short time annealing increased for larger binder content.

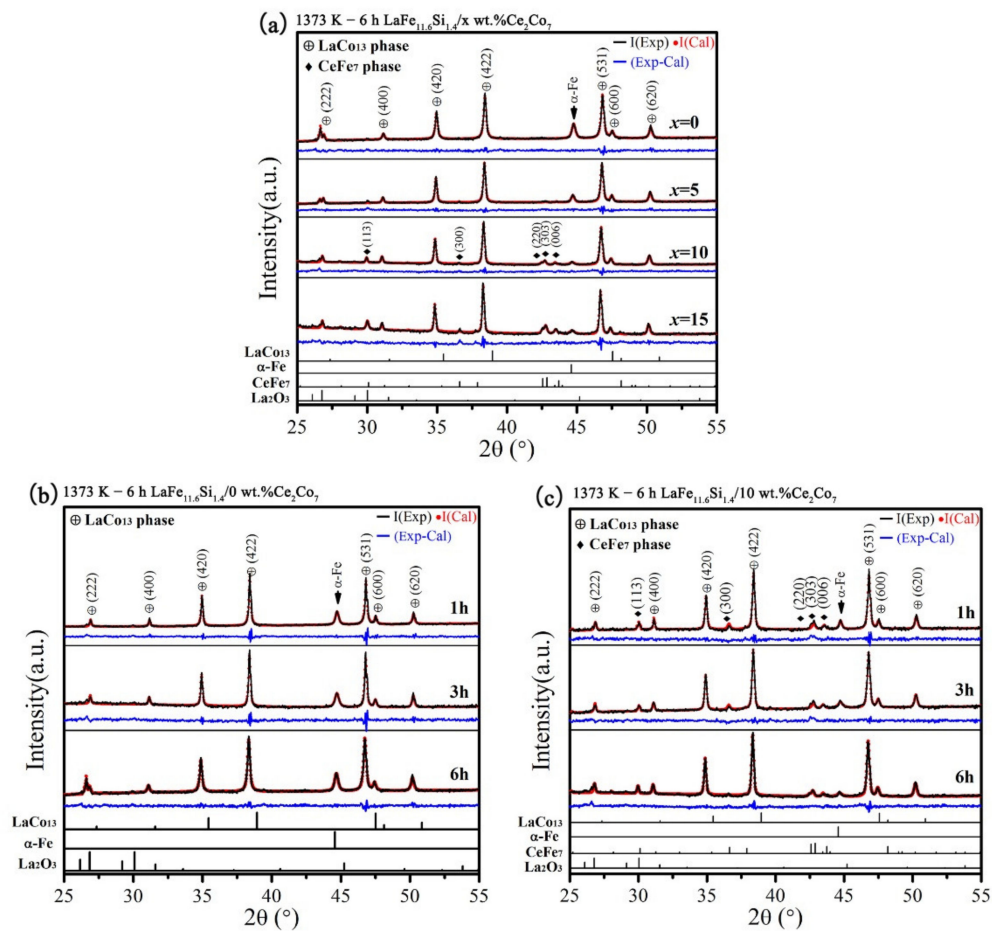


Figure 1. (a) XRD patterns for $\text{LaFe}_{11.6}\text{Si}_{1.4}/x$ wt.% Ce_2Co_7 ($x = 0, 5, 10$ and 15) composites sintered at 1373 K for 6 h ; (b) XRD patterns for binder-free $\text{LaFe}_{11.6}\text{Si}_{1.4}$ composites sintered at 1373 K for $1, 3$ and 6 h , respectively; (c) XRD patterns for $\text{LaFe}_{11.6}\text{Si}_{1.4}/10$ wt.% Ce_2Co_7 composites sintered at 1373 K for $1, 3$ and 6 h , respectively.

Table 1. The weight percentages of phases in the $\text{LaFe}_{11.6}\text{Si}_{1.4}/x$ wt.% Ce_2Co_7 ($x = 0, 5, 10$ and 15) sintered composites and fit coefficient.

Sample	Sintering@1373 K	Weight Percentage (wt.%)			Fit Coefficient					
		1:13 phase	α -Fe Phase	1:7 Phase	R_p	R_{wp}	R_{exp}	χ^2		
Annealed $\text{LaFe}_{11.6}\text{Si}_{1.4}$ flakes		84.69(5)	15.31(2)		0.95	1.62	0.80	4.16		
$\text{LaFe}_{11.6}\text{Si}_{1.4}/x$ wt.% Ce_2Co_7 composites	$x = 0$	1 h	89.36(5)	10.64(2)	/	0.95	1.44	1.10	1.71	
		3 h	87.74(5)	12.26(2)	/	1.28	1.73	1.42	1.49	
		6 h	89.26(5)	10.82(2)	/	0.87	1.36	1.01	1.80	
	$x = 5$	6 h	93.21(5)	5.90(1)	0.89	0.87	1.20	1.01	1.43	
		$x = 10$	1 h	87.28(5)	4.72(1)	8.00	1.08	1.46	1.26	1.33
			3 h	87.02(5)	6.28(1)	6.70	0.98	1.27	1.23	1.07
	$x = 15$	6 h	93.93(5)	3.30(1)	2.77	0.90	1.19	0.98	1.46	
		6 h	88.29(5)	4.96(1)	6.75	1.19	1.53	1.09	1.98	

To investigate the kinetics of diffusion mode of Ce and Co, binder-free and 10 wt.% Ce_2Co_7 composites sintered at 1373 K for $1, 3$ and 6 h were prepared. The Rietveld refined XRD patterns are shown in Figure 1b,c, respectively. The weight percentages of the phases obtained from the Rietveld refined XRD data are listed in Table 1. The phase composition of annealed $\text{LaFe}_{11.6}\text{Si}_{1.4}$ flakes was $84.69(5)$ wt.% 1:13 phase, and $15.31(2)$ wt.% α -Fe phase. There were no peaks of the La_2O_3 , LaFeSi (1:1:1), and $(\text{La,Ce})_2(\text{Fe,Co,Si})_{17}$ (2:17) phases

(Figure 1) in the XRD patterns due to the limitation of the resolution of normal XRD, indicating the low content of these phases in the sintered composites.

Compared with the annealed flakes, the 1:13 phase content in the binder-free sample sintered at 1373 K for 1~6 h (Figure 1b) slightly increased, accompanied by a decrease in α -Fe phase content. This indicated that additional formation of the 1:13 phase occurred during sintering. The XRD patterns of $\text{LaFe}_{11.6}\text{Si}_{1.4}/10 \text{ wt.}\% \text{Ce}_2\text{Co}_7$ composites sintered at 1373 K for 1, 3 and 6 h are displayed in Figure 1c. When the sintering time was extended from 1 h to 6 h, the 1:7 phase content reduced from 8.00 wt.% to 2.77 wt.% (Table 1), indicating that increased high-temperature sintering time can significantly reduce the 1:7 phase content.

3.2. Microstructure Evolution

The microstructure of the composites sintered at 1373 K for 6 h is shown in Figure 2 for various values of Ce_2Co_7 binder content. For the binder-free sample, the black area is the α -Fe phase, the dark gray area is the 1:13 phase (matrix phase), and white grains consist of the La_2O_3 phase (not detected in the XRD results owing to its low mass fraction). After sintering at 1373 K for 6 h, a high mass fraction of the 1:13 phase and a small α -Fe phase content (Table 1) were obtained. It was reported that the temperature range for thermal decomposition (TD) reaction for $\text{La}(\text{Fe},\text{Si},\text{Co})_{13}$ based compounds is 873–1173 K [42]. A lamellar structure, usually observed upon decomposition of the 1:13 phase was not seen, indicating no decomposition of the 1:13 phase occurred during sintering of the binder-free $\text{LaFe}_{11.6}\text{Si}_{1.4}$ composites [43]. The sintering temperature was near the formation temperature of the 1:13 phase, thus, a large amount of precipitation was observed (Figure 2b). The α -Fe phase (black areas), the LaFeSi (1:1:1) phase (white grains inside the 1:13 particles) and the La_2O_3 phase (white grains besides the α -Fe phase), shown in Figure 2b, were observed. As previously reported [42,43], the white phase at the particle interfaces (Figure 2a) is believed to be a La- and Si-rich phase.

From the Ce-Co binary phase diagram [44], the melting point of Ce_2Co_7 alloy is 1418 K, which is 45 K higher than the sintering temperature (1373 K). Therefore, the soft Ce_2Co_7 alloy binder and $\text{LaFe}_{11.6}\text{Si}_{1.4}$ particles could be bonded by solid phase sintering to obtain a highly dense microstructure under a pressure of 30 MPa [45,46].

For the $\text{LaFe}_{11.6}\text{Si}_{1.4}/5 \text{ wt.}\% \text{Ce}_2\text{Co}_7$ sintered composites (Figure 2c,d), the fraction of α -Fe phase (black area), La- and Si-rich boundary phase and La_2O_3 phase (white area) decreased markedly. A small amount of CeFe_7 -type phase (light grey) appeared in the binder bonded composites. The formation enthalpy of CeCo_7 (-10.704 kJ/mol calculated by the modified Miedema (ZSL's Model) [36] is more negative than that of LaCo_{13} (-5.79 kJ/mol) [34], favoring the formation of the 1:7 phase. The EDS map results of the $\text{LaFe}_{11.6}\text{Si}_{1.4}/5 \text{ wt.}\% \text{Ce}_2\text{Co}_7$ sintered composites are shown in the inset of Figure 2c, uniform diffusion of Co occurred in the 1:13 phase. However, there are some regions of La and Ce enrichment, accompanied by up to ~68 at.% for oxygen (Figure 2d). Owing to the limitation of EDS in quantifying the concentration of light elements, this value for oxygen must be regarded as a rough estimate. These La- and Ce-rich regions can correspond to the $(\text{La},\text{Ce})_2\text{O}_3$ phase. Ce is mainly found in the 1:7 phase, a small amount of Ce is found in the 1:13 phase. Sintering at 1373 K for 6 h cannot produce a uniform distribution of Ce or eliminate the 1:7 phase.

Interestingly, the LaFeSi (1:1:1), La-, and Si-rich phases are virtually absent in $\text{LaFe}_{11.6}\text{Si}_{1.4}/x \text{ wt.}\% \text{Ce}_2\text{Co}_7$ ($x = 5, 10, 15$) composites sintered at 1373 K for 6 h. The chemical compositions of the 1:7 and 1:13 phases and lattice constant (a) of 1:13 phase for the sintered composites are listed in Table 2. The 1:13 phase, with a composition of $\text{La}_{0.87}\text{Ce}_{0.13}\text{Fe}_{9.70}\text{Co}_{0.56}\text{Si}_{1.35}$, $\text{La}_{0.82}\text{Ce}_{0.18}\text{Fe}_{9.24}\text{Co}_{0.91}\text{Si}_{1.34}$, and $\text{La}_{0.75}\text{Ce}_{0.25}\text{Fe}_{9.10}\text{Co}_{1.30}\text{Si}_{1.28}$ was obtained in sintered composites with 5 wt.%, 10 wt.%, and 15 wt.% Ce_2Co_7 , respectively.

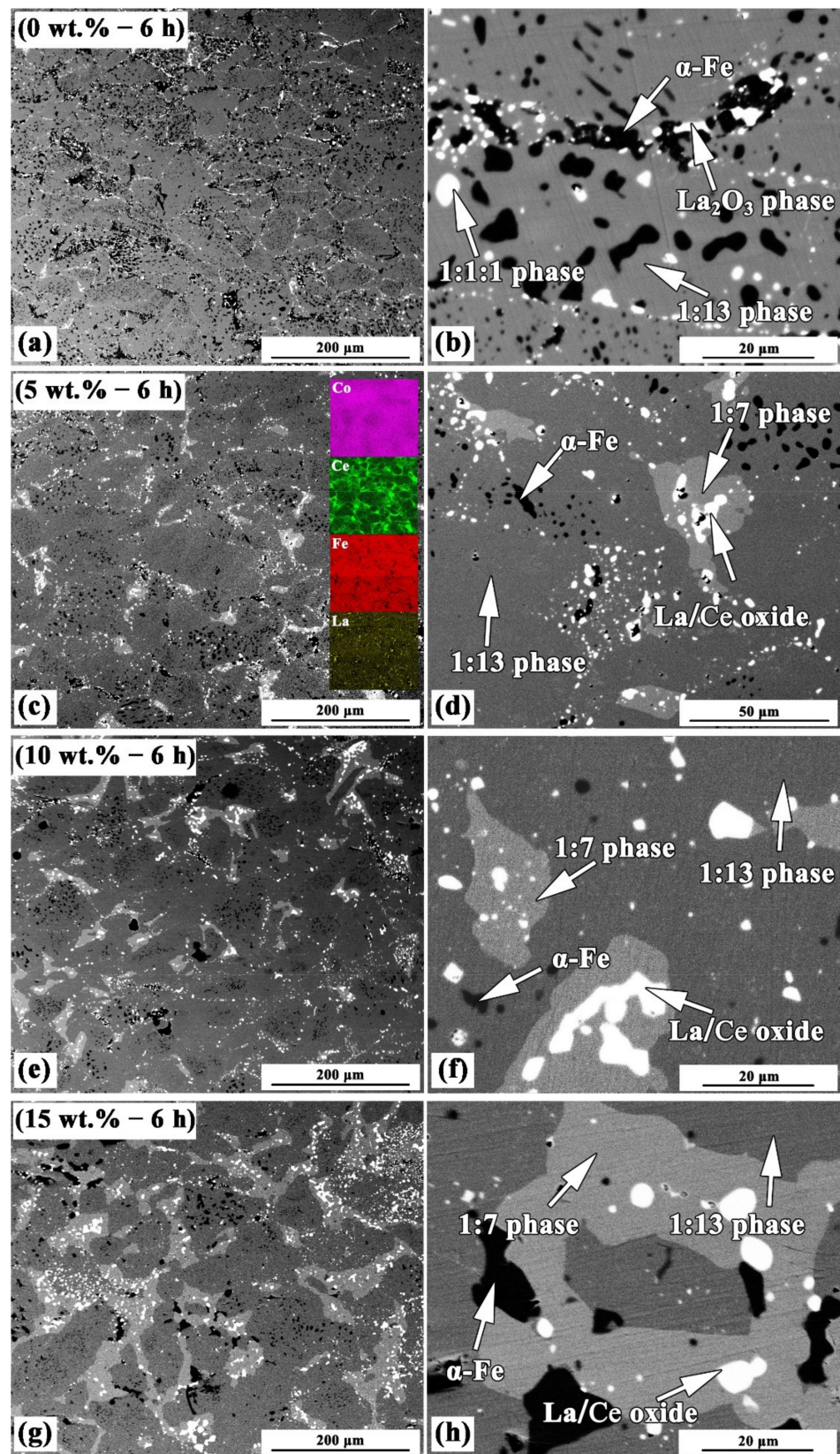


Figure 2. Backscattered SEM micrographs of $\text{LaFe}_{11.6}\text{Si}_{1.4}/x$ wt.% Ce_2Co_7 composites with $x = 0$ (a,b), 5 (c,d), 10 (e,f), and 15 (g,h) sintered at 1373 K for 6 h, respectively. The inset of (c) shows the mapping results of La, Ce, Fe and Co elements for $\text{LaFe}_{11.6}\text{Si}_{1.4}/5$ wt.% Ce_2Co_7 composites sintered at 1373 K for 6 h, respectively.

Table 2. Lattice constant (a), phase composition, Curie temperature (T_C), maximum magnetic entropy change ($(-\Delta S_M)^{\max}$), and relative cooling power (RCP) of $\text{LaFe}_{11.6}\text{Si}_{1.4}/x$ wt.% Ce_2Co_7 ($x = 0, 5, 10$ and 15) composites sintered at 1373 K for 1~6 h.

LaFe _{11.6} Si _{1.4} /Ce ₂ Co ₇ Composites		Phase Composition		T_C (K)	$(-\Delta S_M)^{\max}$ J/(kg·K) $\Delta H = 2 \text{ T (5 T)}$	RCP J/kg $\Delta H = 2 \text{ T (5 T)}$	
Binder Content	Sintering	1:13 Phase a (Å)	1:7 Phase				1:13 Phase
Binder-free	1373 K/1 h	11.49282(6)	—	LaFe _{10.95} Si _{1.59}	206	7.5 (/)	122.4 (/)
	1373 K/3 h	11.49015(9)	—	LaFe _{10.73} Si _{1.57}	210	5.0 (/)	106.6 (/)
	1373 K/6 h	11.49209(9)	—	LaFe _{10.53} Si _{1.60}	212	5.2 (8.8)	146.7 (339.0)
5 wt.%	1373 K/6 h	11.49190(0)	La _{0.26} Ce _{0.74} Fe _{6.02} Co _{0.56} Si _{0.93}	La _{0.87} Ce _{0.13} Fe _{9.70} Co _{0.56} Si _{1.35}	247	4.0 (8.6)	158.4 (428.7)
	1373 K/1 h	11.49271(9)	La _{0.28} Ce _{0.72} Fe _{5.75} Co _{1.27} Si _{0.87}	La _{0.89} Ce _{0.11} Fe _{9.71} Co _{0.91} Si _{1.35}	275	0.9 (/)	—
10 wt.%	1373 K/3 h	11.49559(8)	La _{0.27} Ce _{0.73} Fe _{6.14} Co _{0.82} Si _{0.90}	La _{0.83} Ce _{0.17} Fe _{9.82} Co _{0.95} Si _{1.29}	296	2.2 (/)	185.2 (/)
	1373 K/6 h	11.49301(7)	La _{0.27} Ce _{0.73} Fe _{6.32} Co _{0.72} Si _{1.04}	La _{0.82} Ce _{0.18} Fe _{9.24} Co _{0.91} Si _{1.34}	291	3.9 (7.6)	209.2 (457.7)
15 wt.%	1373 K/6 h	11.51400(9)	La _{0.28} Ce _{0.72} Fe _{5.71} Co _{0.98} Si _{0.91}	La _{0.75} Ce _{0.25} Fe _{9.10} Co _{1.30} Si _{1.28}	331	3.2 (6.0)	178.3 (399.2)

On the other hand, in sintered composites with 10 wt.% and 15 wt.% Ce_2Co_7 , the fraction of 1:7 phase (light gray) increased remarkably, accompanied by a decrease in the α -Fe phase content. With 10 wt.% Ce_2Co_7 , the content of Ce and Co in the 1:13 phase reached 1.34 at.% and 7.51 at.%, respectively. With 15 wt.% Ce_2Co_7 , the values of Ce and Co content in the 1:13 phase matrix were 1.89 at.% and 10.26 at.%, respectively. This change in the composition of the 1:13 phase illustrates that diffusion of Ce and Co increased for larger Ce_2Co_7 binder content. The lattice parameter a of the 1:13 phase is similar in the sintered samples with 0–10 wt.% Ce_2Co_7 . However, the a of the 1:13 phase increased for 15 wt.% Ce_2Co_7 samples. For the 1:7 phase, the Co content increased while the Ce fraction in the 1:7 phase was almost unchanged with increasing Ce_2Co_7 content. The 1:7 phase is an iron-poor type 2:17 phase, these two phases have the same crystal structure [47]. For the 2:17 phase in the composite, the atom ratio of (Fe + Co + Si) to (La + Ce) is 8.5. The EDS results of the 1:7 phase include the contribution from the 2:17 phase, thus the ratio is not always equal to 7 (Table 2).

3.3. Kinetics of Diffusion of Ce and Co

To understand the diffusion of Ce and Co, the binder-free and 10 wt.% Ce_2Co_7 composites were studied. Backscattered SEM micrographs of the composites with and without 10 wt.% Ce_2Co_7 sintered at 1373 K for 1, 3, and 6 h are shown in Figure 3. For the binder-free samples (Figure 3a–c), with increasing sintering time from 1 to 6 h, the grain boundaries (white phase) are more obvious. It is likely that a La- and Si-rich phase formed at the particle boundaries of the 1:13 phase during sintering [43], similar to the microstructure of $\text{Nd}_2\text{Fe}_{14}\text{B}$ magnets produced by liquid phase sintering (LPS). Sintering occurred at approximately the temperature of 1:13 phase formation, resulting in 1:13 phase formation [20]. The La- and Si-rich phases were distributed at particles boundaries while the α -Fe phase was inside the 1:13 particles [42]. The fraction of α -Fe phase in the 1:13 particles decreased, while the size of the α -Fe phase grains increased. The EDS results show that the content of Fe in the 1:13 phase matrix decreased, indicating that the 1:13 phase formed in the binder-free samples by the following reaction [48]:



For the 10 wt.% Ce_2Co_7 samples (Figure 3d–f), the content of the 1:7 and α -Fe phases reduced with increasing sintering time, which is consistent with the results in Figure 1 and Table 1. The α -Fe phase in the 1:13 phase reduced and eventually disappeared with increasing sintering time. The increase of Ce, Co content in the 1:13 phase (Table 2) indicated that Ce, Co diffusion increased for larger sintering time. As sintering time increased, the α -Fe phase content decreased while the content of Fe in the 1:7 phase increased. In sintered composites with 10 wt.% Ce_2Co_7 binder, the ratio of (La,Ce) to (Fe,Co,Si) in the 1:13 phase was higher than that of binder-free samples.

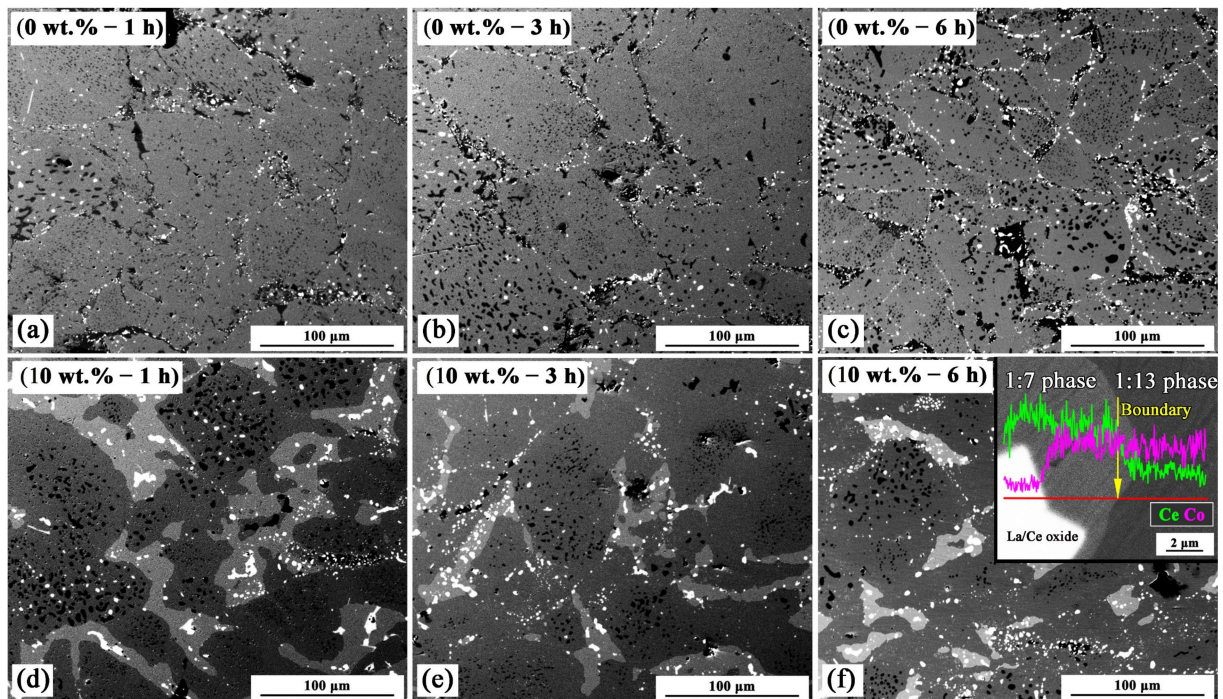


Figure 3. Backscattered SEM micrographs of binder-free $\text{LaFe}_{11.6}\text{Si}_{1.4}$ composites (a–c) and $\text{LaFe}_{11.6}\text{Si}_{1.4}/10 \text{ wt.}\% \text{Ce}_2\text{Co}_7$ composites (d–f) sintered at 1373 K for 1, 3 and 6 h, respectively. The inset of Fig.3(f) shows the line scan results of the interphase boundary between the 1:13 phase and the 1:7 phase for $\text{LaFe}_{11.6}\text{Si}_{1.4}/10 \text{ wt.}\% \text{Ce}_2\text{Co}_7$ composites sintered at 1373 K for 6 h.

In the $\text{La}(\text{Fe},\text{Si})_{13}$ unit cell, La atoms occupy 8a sites, Fe atoms occupy 8b (FeI) and 96i (FeII) positions in the ratio of 1:12. Si atoms occupy Fe positions [49,50]. The similar electronic structure of Co and Fe atoms or Ce and La atoms implies that Co atoms will occupy the position of FeII atoms, and Ce atoms will substitute the position of La atoms. In all Ce_2Co_7 bonded sintered composites, the relative atomic content of La and Ce atoms for the 1:7 phase remains unchanged at $\sim 27:73$, but the relative content of Co, Fe, and Si is changed (Table 2). The SEM micrographs of composites with 10 wt.% Ce_2Co_7 sintered at 1373 K for 6 h is shown in the inset of Figure 3f. The line scan of the interphase boundary between the 1:13 phase and the 1:7 phase showed a sudden change in Ce content and little change in Co concentration. Thus, the diffusion of Ce and Co in the 1:13 phase occurs by different mechanisms. Co diffuses by the usual vacancy diffusion mechanism in the 1:13 phase. On the other hand, Ce diffusion is by reaction diffusion. The Ce content in the 1:13 phase is mainly due to the reaction between the Ce-rich $(\text{La},\text{Ce})(\text{Fe},\text{Co},\text{Si})_7$ phase and the $\text{La}(\text{Fe},\text{Co},\text{Si})_{13}$ phase, resulting in the formation of $(\text{La},\text{Ce})(\text{Fe},\text{Co},\text{Si})_{13}$ phase. Therefore, Ce is mainly enriched in 1:7 phase but Co is uniformly distributed.

3.4. Thermal Conductivity, Mechanical and Magnetic Properties

The thermal conductivity of the studied samples in this work was measured at room temperature. The porosity, thermal conductivity, and mechanical properties (Figure 4) of the $\text{LaFe}_{11.6}\text{Si}_{1.4}/x \text{ wt.}\% \text{Ce}_2\text{Co}_7$ ($x = 0, 5, 10, \text{ and } 15$) composites sintered at 1373 K for 6 h are listed in Table 3. For the $\text{LaFe}_{11.6}\text{Si}_{1.4}/x \text{ wt.}\% \text{Ce}_2\text{Co}_7$ ($x = 0, 5, 10, \text{ and } 15$) composites, structures with density up to 95% were successfully obtained. This high density resulted in a high value of compressive strength (σ_{bc}^{max}) of up to 450 MPa and high thermal conductivity of up to 7.5 W/m·K. These composites exhibited markedly higher (σ_{bc}^{max}) value than those of low melting point alloy bonded composites fabricated by low temperature hot pressing (200 MPa) [32].

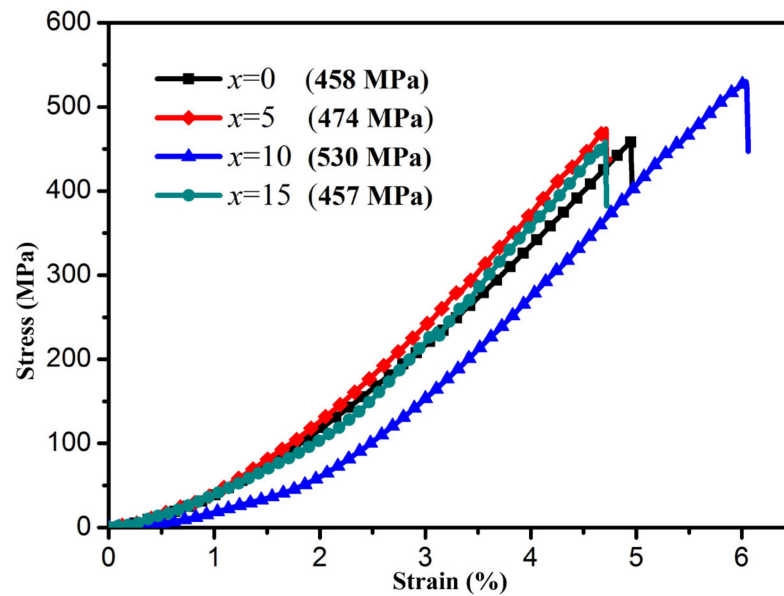


Figure 4. Stress–strain curves for the $\text{LaFe}_{11.6}\text{Si}_{1.4}/x$ wt.% Ce_2Co_7 ($x = 0, 5, 10$ and 15) composites sintered at 1373 K for 6 h.

Table 3. Porosity, thermal conductivity, and mechanical properties of $\text{LaFe}_{11.6}\text{Si}_{1.4}/x$ wt.% Ce_2Co_7 ($x = 0, 5, 10$ and 15) composites sintered at 1373 K for 6 h.

Sample	Porosity (%)	λ (W/m·K)	$(\sigma_{bc})^{\max}$ (MPa)	Strain (%)
Binder free	5.14	13.71	458	5.0
5 wt.%	4.02	7.81	474	4.7
10 wt.%	4.78	8.21	530	6.1
15 wt.%	4.56	7.50	457	4.7

The thermal conductivity of these composites are comparable or larger than the values for hot-pressed $\text{La}_{0.7}\text{Ce}_{0.3}\text{Fe}_{11.45}\text{Mn}_{0.15}\text{Si}_{1.4}/13.5\%$ Fe (7.5 W/m·K) [51] and $\text{LaFe}_{11.6}\text{Si}_{1.4}\text{H}_y/\text{Sn}$ (7.9 W/m·K) [32], but smaller than those of hot-pressed $\text{La}_{0.8}\text{Ce}_{0.2}(\text{Fe}_{0.95}\text{Co}_{0.05})_{11.8}\text{Si}_{1.2}/\text{Sn}_{42}\text{Bi}_{58}$ (10.72 – 19.64 W/m·K) [33], $\text{LaFe}_{11}\text{Co}_{0.8}\text{Si}_{1.2}/\text{Al}$ (9.9 – 17.0 W/m·K) [52], and $\text{La}_{0.7}\text{Ce}_{0.3}\text{Fe}_{11.48}\text{Mn}_{0.12}\text{Si}_{1.4}\text{H}_{1.8}/20$ wt.%In (11.5 W/m·K) [53]. As $\text{La}(\text{Fe},\text{Si})_{13}$ and residual Ce-Co phase possess different thermal conductivities, thermal conductivity of sintered composites may be improved by even longer sintering time. The strain values are larger than 4.7% , which is about 4.5 times the values of sintered $\text{LaFe}_{11.7}\text{Co}_{1.3}\text{Si}$ composites [42]. Thus, the ductility of the $\text{LaFe}_{11.6}\text{Si}_{1.4}/x$ wt.% Ce_2Co_7 ($x = 0, 5, 10$ and 15) composites sintered at 1373 K for 6 h is markedly improved. These improved properties are mainly due to the stress distribution in the α -Fe and $1:7$ phases and the improved quality of the sintered compacts during high temperature sintering. High ultimate compressive stress and better elongation can lead to better machinability.

The normalized $M_{\text{norm}}-T$ ($M/M_{\text{max}}-T$) curves upon cooling process under 0.05 T, normalized magnetization temperature derivative curves ($dM_{\text{norm}}/dT-T$) measured during cooling under an applied field of 0.05 T and the $(-\Delta S_M)-T$ curves measured under applied field changes of 0 – 2 and 0 – 5 T for the $\text{LaFe}_{11.6}\text{Si}_{1.4}/x$ wt.% Ce_2Co_7 ($x = 0, 5, 10$ and 15) composites sintered at 1373 K for 6 h are shown in Figures 5 and 6, respectively. The isothermal magnetization curves for the $\text{LaFe}_{11.6}\text{Si}_{1.4}/x$ wt.% Ce_2Co_7 were measured with an increasing magnetic field in a wide temperature range. The sweep rate of the field was slow enough to ensure that the data were recorded in an isothermal process. The value of the isothermal magnetic entropy change $-\Delta S_M(T, H)$ is given by the Maxwell relationship:

$$-\Delta S_M(T, H) = \int_0^H (\partial M / \partial T) dH \quad (2)$$

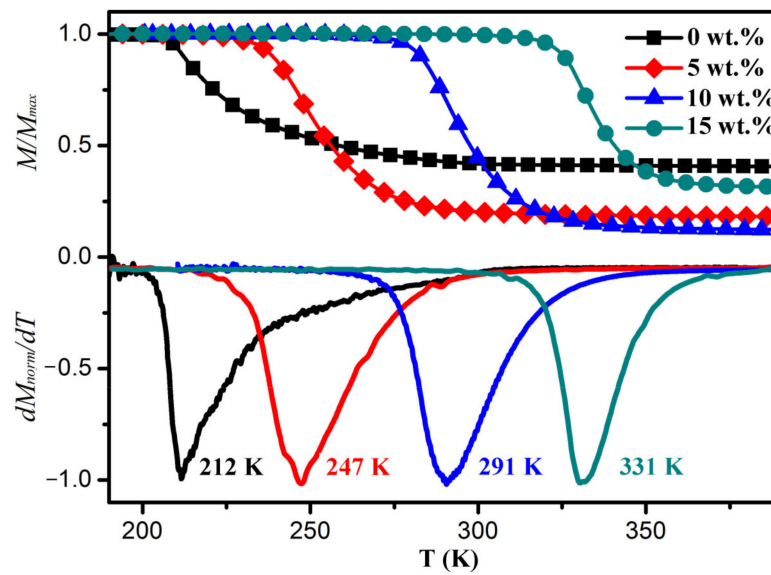


Figure 5. Normalized M/M_{max} - T and dM_{norm}/dT - T curves of $\text{LaFe}_{11.6}\text{Si}_{1.4}/x$ wt.% Ce_2Co_7 ($x = 0, 5, 10$, and 15) composites sintered at 1373 K for 6 h upon cooling under an applied field of 0.05 T.

Another parameter called RCP (Relative Cooling Power) can be employed to evaluate the refrigeration efficiency. RCP was defined as the product of $(-\Delta S_M)^{max}$ times the full temperature width at half maximum of the peak ($\text{RCR} = (-\Delta S_M)^{max} \times \delta T_{FWHM}$) [54]. The values of T_C , $(-\Delta S_M)^{max}$ and RCP of the studied composites are presented in Table 2.

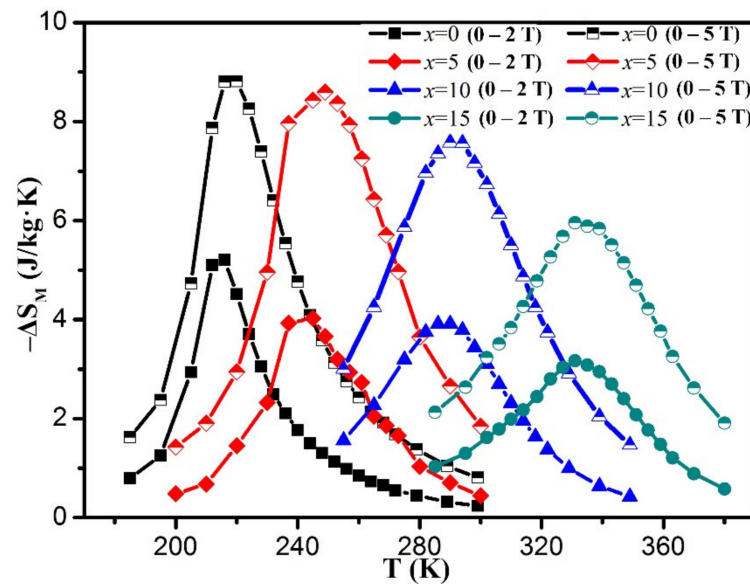


Figure 6. Magnetic entropy change $(-\Delta S_M)$ as function of temperature for the $\text{LaFe}_{11.6}\text{Si}_{1.4}/x$ wt.% Ce_2Co_7 ($x = 0, 5, 10$ and 15) composites sintered at 1373 K for 6 h.

The binder-free sintered composites show higher T_C (212 K) than that of the annealed $\text{LaFe}_{11.6}\text{Si}_{1.4}$ flakes (196 K). The sintering temperature is close to the optimum formation temperature of the $1:13$ phase [55], which may bring about $1:13$ phase formation and decrease the α -Fe phase content (Table 1), resulting in the formation of a nonstoichiometric Fe deficient $1:13$ phase (Table 2). This Fe-deficient $1:13$ phase has elevated T_C (Table 2), which weakens the first order magnetic transition (FOMT) and lowers the $(-\Delta S_M)^{max}$ [7,18,34]. The binder-free composites exhibited the maximum magnetic entropy change $(-\Delta S_M)^{max}$ of 5.2 and 8.8 J/kg·K under applied field changes of 0 - 2 and 0 - 5 T, respectively (Table 2).

The T_C of the $\text{LaFe}_{11.6}\text{Si}_{1.4}/x$ wt.% Ce_2Co_7 ($x = 5, 10,$ and 15) composites increased linearly with larger Ce_2Co_7 content due to the higher Co content diffused into the 1:13 phase. Sintering caused Ce and Co to diffuse from the Ce_2Co_7 binder to the 1:13 particles through the particle boundaries. It changed the chemical composition of the 1:13 phase, the 1:13 phase content, and the magnetocaloric performance. As calculated from the results in Table 2, the content of Ce and Co in the 1:13 phase increased from 1.03 to 1.97 at.% and 4.44 to 10.25 at.%, respectively. The T_C of sintered composites increased from 247 K to 331 K due to the substitution of Fe by Co in the 1:13 phase. Under the applied field changes of 2 T and 5 T, the $(-\Delta S_M)^{\text{max}}$ values of the $\text{LaFe}_{11.6}\text{Si}_{1.4}/x$ wt.% Ce_2Co_7 composites with $x = 0, 5, 10$ and 15 were 5.2, 4.0, 3.9, 3.2 J/kg·K and 8.8, 8.6, 7.6, 6.0 J/kg·K, respectively. RCP values of these composites were 146.7, 158.4, 209.2, and 178.3 J/kg and 339.0, 428.7, 457.7, and 399.2 J/kg, respectively (Table 2).

Interestingly, the $(-\Delta S_M)^{\text{max}}$ (~ 5.2 J/kg·K@2 T at 212 K) of the binder-free composite was larger than that of the $\text{LaFe}_{11.6}\text{Si}_{1.4}$ bulk composite with particle size smaller than 100 μm (~ 4.0 J/kg·K@2 T at 220 K) [56], and far larger than that of $\text{La}(\text{Fe},\text{Co})_{11.4}\text{Al}_{1.6}$ alloy (2.2 J/kg·K@2 T at 205 K) [50] in a similar temperature range. The $(-\Delta S_M)^{\text{max}}$ value (~ 4 J/kg·K@2 T at 247 K) of the composite with 5 wt.% Ce_2Co_7 binder was larger than those of $\text{LaFe}_{11.6}\text{Si}_{1.4}/5$ wt.% $\text{Pr}_{40}\text{Co}_{60}$ (~ 2.9 J/kg·K@2 T at 247 K) [56] and $\text{Gd}_{50}\text{Co}_{48}\text{Zn}_2$ as-spun ribbons [57] (2.6 J/kg·K@2 T at 260 K) in a similar temperature range. Compared with Gd [58], the values of $(-\Delta S_M)^{\text{max}}$ (~ 3.9 J/kg·K@2 T at 291 K) and RCP (209.2 J/kg@2 T) of the $\text{LaFe}_{11.6}\text{Si}_{1.4}/10$ wt.% Ce_2Co_7 composite is smaller. For an applied field change of 2 T, the values of $(-\Delta S_M)^{\text{max}}$ and RCP for the $\text{LaFe}_{11.6}\text{Si}_{1.4}/15$ wt.% Ce_2Co_7 composite (Table 2) are much larger than those of $\text{Fe}_{77}\text{Ta}_3\text{B}_{10}\text{Zr}_9\text{Cu}_1$ amorphous ribbons ($(-\Delta S_M)^{\text{max}} \sim 1.47$ J/kg·K@2 T at 336 K; RCP ~ 123.9 J/kg) in the similar temperature [59].

The Arrott plots near T_C of the $\text{LaFe}_{11.6}\text{Si}_{1.4}/x$ wt.% Ce_2Co_7 ($x = 0, 5, 10$ and 15) composites sintered at 1373 K for 6 h are shown in Figure 7. According to the Banerjee criterion [60], the slopes of the Arrott plots for the composites sintered at 1373 K for 6 h are all positive. The magnetic phase transition of these sintered composites near its T_C is a second-order magnetic phase transition, which is due to Co diffusion in Ce_2Co_7 bonded composites and enrichment of Si in the 1:13 matrix for the binder-free composite. A similar behavior was observed for the binder-free and 10 wt.% Ce_2Co_7 binder composites sintered at 1373 K for 1~6 h, which also exhibited a second-order magnetic phase transition near their T_C .

The normalized $M/M_{\text{max}}-T$ curves upon cooling under an applied field of 0.05 T of the binder-free and 10 wt.% Ce_2Co_7 binder composites sintered at 1373 K are shown in Figure 8. The $(-\Delta S_M)-T$ curves (0 – 2 T) are shown in the inset of Figure 8, respectively. For the binder-free composites, there is a composition change of the magnetocaloric phase (1:13 phase) after sintering. Based on earlier work [61], the decrease of Fe/Si ratio in 1:13 phase results in higher T_C and lower $-\Delta S_M$. With increasing annealing time from 1 to 6 h, the Fe/Si ratio in the binder-free composites decreased from ~ 6.89 (10.95/1.59) to ~ 6.58 (10.53/1.60), the T_C increased from ~ 206 to 212 K while $(-\Delta S_M)^{\text{max}}$ decreased from 7.5 to 5.2 J/kg·K ($\Delta H = 2$ T) (Table 2). The 10 wt.% Ce_2Co_7 binder composites also exhibited higher $(-\Delta S_M)^{\text{max}}$ due to the diffusion of Ce, which increased the Ce content in the 1:13 phase. Hence, the change of T_C and magnetocaloric properties is attributed to the formation of the 1:13 phase (Table 1) and grain boundary diffusion of Ce and Co atoms.

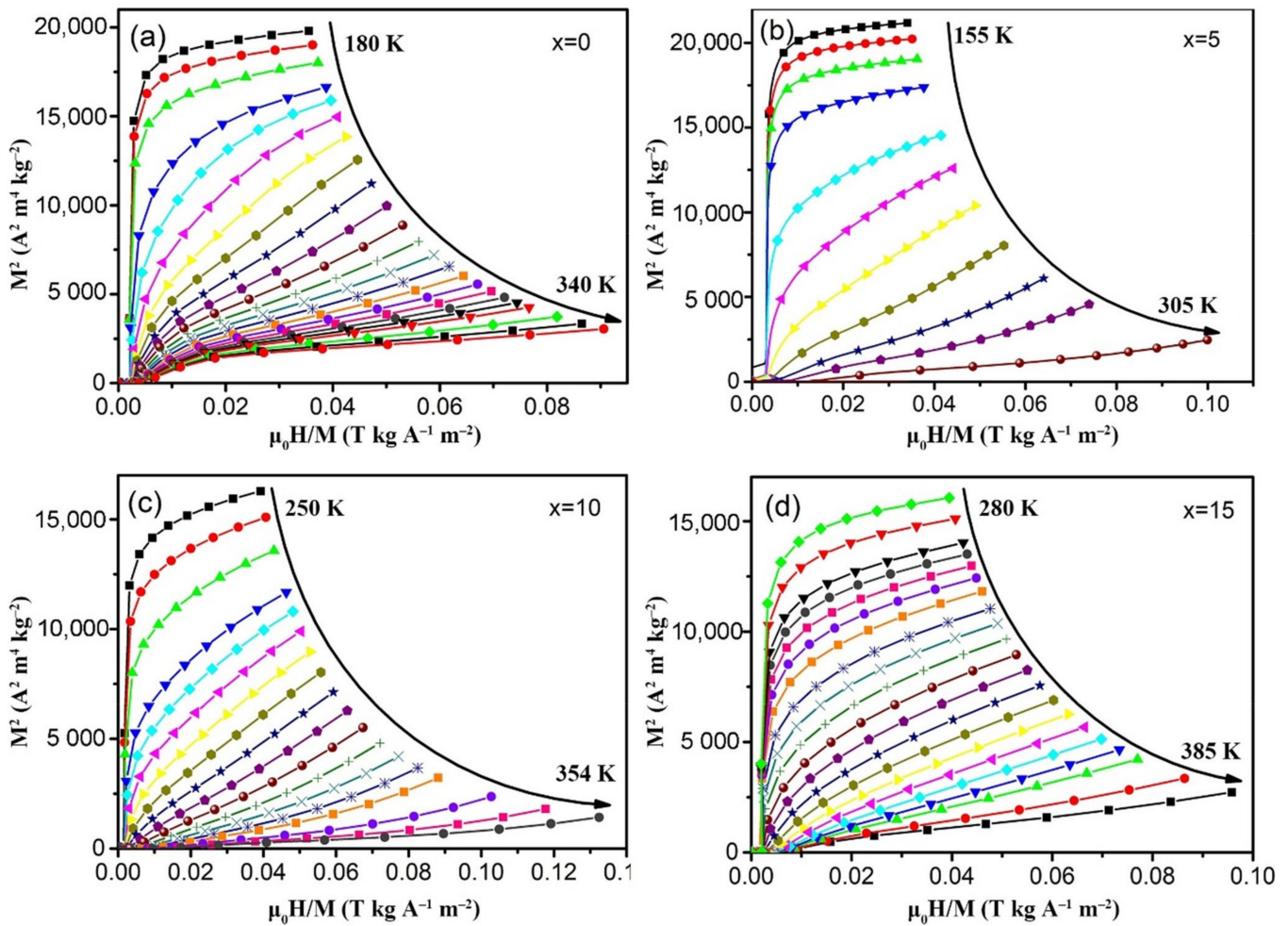


Figure 7. Arrott plots (a–d) of the $\text{LaFe}_{11.6}\text{Si}_{1.4}/x\text{wt.}\% \text{Ce}_2\text{Co}_7$ ($x = 0, 5, 10,$ and 15) composites sintered at 1373 K for 6 h .

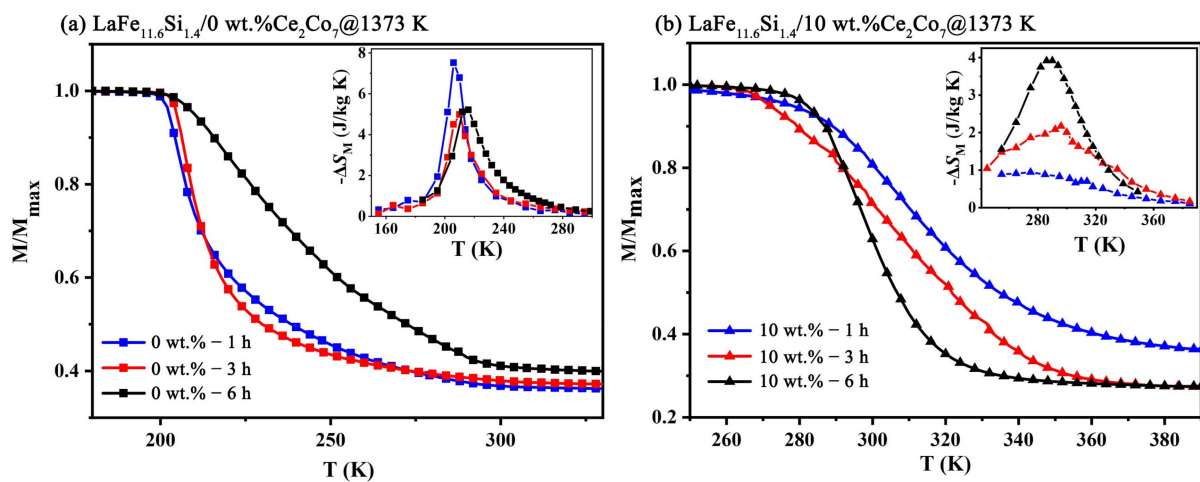


Figure 8. Normalized $M/M_{\text{max}}-T$ curves of the binder-free and $10 \text{ wt.}\% \text{Ce}_2\text{Co}_7$ binder composites sintered at 1373 K for $1\text{--}6 \text{ h}$ upon cooling under an applied field of 0.05 T . Insets in panels (a,b) are $(-\Delta S_M)$ vs. T curves for the composites with and without Ce_2Co_7 binder under a magnetic field change of $0\text{--}2 \text{ T}$, respectively.

4. Conclusions

In summary, the diffusion of Ce and Co into the desired $(\text{La,Ce})(\text{Fe,Co,Si})_{13}$ phase and the partial substitution of La by Ce and Fe by Co could be realized by a one-step sintering of $\text{La}(\text{Fe,Si})_{13}/\text{Ce-Co}$ composites. The line scan of the interphase boundary between the 1:13 phase and the 1:7 phase showed a sudden change in Ce content and little change in Co concentration. Thus, the diffusion mechanism of Ce in the 1:13 phase was different from that of Co. Co diffused by the usual vacancy diffusion mechanism while the diffusion mode of Ce was by reaction diffusion. After 6 h sintering at 1373 K, a high value of compressive strength $(\sigma_{bc})^{\max}$ of up to 450 MPa and a high thermal conductivity (λ) of up to 7.5 W/m·K were successfully obtained. The magnetocaloric properties of the composites could also be tuned by varying the content of Ce-Co alloy binder and the sintering time. T_C increased from 212 K to 331 K with increasing Ce_2Co_7 from 0 to 15 wt.% in $\text{LaFe}_{11.6}\text{Si}_{1.4}/\text{Ce-Co}$ bulk composites. The magnetic entropy change decreased from 8.8 to 6.0 J/kg·K, the relative cooling power increased from ~339 to 428, 457 J/kg and then decreases to 399 J/kg under 5 T.

Thus, a feasible route to produce high quality $\text{La}(\text{Fe,Si})_{13}$ based magnetocaloric composites with large MCE, good mechanical properties and thermal conductivity and tunable T_C by a one-step sintering process has been demonstrated.

Author Contributions: Conceptualization, Methodology, Supervision, Writing—original draft, X.-C.Z.; Conceptualization, Methodology, Formal analysis, Investigation, Data curation, Writing—original draft, X.-T.D.; Software, Resources, Validation, J.-H.H., C.-L.L., H.Z. and Y.-L.H. Visualization, Investigation, Formal analysis, H.-Y.Y.; Writing—review & editing R.V.R. All authors have read and agreed to the published version of the manuscript.

Funding: This work was funded by the National Natural Science Foundation of China (Grant Nos. 51874143, 52066001, 51671022, 51461012), the Natural Science Foundation of Guangdong Province (Grant Nos. 2019A1515010970, 2017A030313317), the National Key Research & Development Program of China (Materials Genome Initiative) (Grant No. 2017YFB0702703), the Guangzhou Municipal Science and Technology Project (Grant No. 201904010030), and the Foundation of State Key Laboratory of Baiyunobo Rare Earth Resource Researches and Comprehensive Utilization (Grant No. 2020Z2218). This Research is also supported by Singapore-HUJ Alliance for Research and Enterprise (SHARE), Nanomaterials for Energy and Energy-Water Nexus (NEW), Campus for Research Excellence and Technological Enterprise (CREATE), Singapore 138602. And the APC was funded by the National Natural Science Foundation of China (Grant No. 51874143).

Institutional Review Board Statement: Not applicable.

Informed Consent Statement: Not applicable.

Data Availability Statement: The data used to support the findings of this study are available from the corresponding author upon request.

Acknowledgments: The authors are grateful to Chun-Ming Li for experimental assistance. The authors wish to also thank Yu-Cai Wu for modifying the figures of this paper.

Conflicts of Interest: The authors declare that they have no known competing financial interests or personal relationships that could have appeared to influence the work reported in this paper.

References

1. Gutfleisch, O.; Willard, M.A.; Brück, E.; Chen, C.H.; Sankar, S.G.; Liu, J.P. Magnetic Materials and Devices for the 21st Century: Stronger, Lighter, and More Energy Efficient. *Adv. Mater.* **2011**, *23*, 821–842. [[CrossRef](#)] [[PubMed](#)]
2. Chaudhary, V.; Chen, X.; Ramanujan, R.V. Iron and manganese based magnetocaloric materials for near room temperature thermal management. *Prog. Mater. Sci.* **2019**, *100*, 64–98. [[CrossRef](#)]
3. Pecharsky, V.K.; Gschneidner, K.A., Jr. Giant Magnetocaloric Effect in $\text{Gd}_5(\text{Si}_2\text{Ge}_2)$. *Phys. Rev. Lett.* **1997**, *78*, 4494–4497. [[CrossRef](#)]
4. Virgil, P.; Alexander, J.S.; Robert, D.S. Reduction of hysteresis losses in the magnetic refrigerant $\text{Gd}_5\text{Ge}_2\text{Si}_2$ by the addition of iron. *Nature* **2004**, *429*, 853–857.
5. Tegus, O.; Brück, E.; Buschow, K.H.J.; De Boer, F.R. Transition-metal-based magnetic refrigerants for room-temperature applications. *Nature* **2002**, *415*, 150–152. [[CrossRef](#)] [[PubMed](#)]

6. Li, Y.; Zeng, Q.Q.; Wei, Z.Y.; Liu, E.K.; Han, X.L.; Du, Z.W.; Li, L.W.; Xi, X.K.; Wang, W.H.; Wang, S.G.; et al. An efficient scheme to tailor the magnetostructural transitions by staged quenching and cyclical ageing in hexagonal martensitic alloys. *Acta Mater.* **2019**, *174*, 289–299. [[CrossRef](#)]
7. Hu, F.X.; Shen, B.G.; Sun, J.R.; Cheng, Z.H.; Rao, G.H.; Zhang, X.X. Influence of negative lattice expansion and meta-magnetic transition on magnetic entropy change in the compound $\text{LaFe}_{11.4}\text{Si}_{1.6}$. *Appl. Phys. Lett.* **2001**, *78*, 3675–3677. [[CrossRef](#)]
8. Fujita, A.; Fujieda, S.; Fukamichi, K.; Mitamura, H.; Goto, T. Itinerant-electron metamagnetic transition and large magneto-volume effects in $\text{La}(\text{Fe}_x\text{Si}_{1-x})_{13}$ compounds. *Phys. Rev.* **2001**, *B65*, 014410. [[CrossRef](#)]
9. Krenke, T.; Duman, E.; Acet, M.; Wassermann, E.F.; Moya, X.; Mañosa, L.; Planes, A. Inverse magnetocaloric effect in ferromagnetic Ni-Mn-Sn alloys. *Nat. Mater.* **2005**, *4*, 450–454. [[CrossRef](#)]
10. Li, L.W.; Xu, P.; Ye, S.K.; Li, Y.; Liu, G.D.; Huo, D.X.; Yan, M. Magnetic properties and excellent cryogenic magnetocaloric performances in B-site ordered $\text{RE}_2\text{ZnMnO}_6$ (RE=Gd, Dy and Ho) perovskites. *Acta Mater.* **2020**, *194*, 354–365. [[CrossRef](#)]
11. Wu, B.B.; Zhang, Y.K.; Guo, D.; Wang, J.; Ren, Z.M. Structure, magnetic properties and cryogenic magneto-caloric effect (MCE) in $\text{RE}_2\text{FeAlO}_6$ (RE=Gd, Dy, Ho) oxides. *Ceram. Int.* **2021**, *47*, 6290–6297. [[CrossRef](#)]
12. Wang, Y.M.; Guo, D.; Wu, B.B.; Geng, S.H.; Zhang, Y.K. Magnetocaloric effect and refrigeration performance in $\text{RE}_{60}\text{Co}_{20}\text{Ni}_{20}$ (RE = Ho and Er) amorphous ribbons. *J. Magn. Magn. Mater.* **2019**, *498*, 166179. [[CrossRef](#)]
13. Ma, Z.P.; Dong, X.S.; Zhang, Z.Q.; Li, L.W. Achievement of promising cryogenic magnetocaloric performances in $\text{La}_{1-x}\text{Pr}_x\text{Fe}_{12}\text{B}_6$ compounds. *J. Mater. Sci. Technol.* **2021**, *92*, 138–142. [[CrossRef](#)]
14. Li, L.W.; Yan, M. Recent progresses in exploring the rare earth based intermetallic compounds for cryogenic magnetic refrigeration. *J. Alloys Compd.* **2020**, *823*, 153810. [[CrossRef](#)]
15. Zou, J.D.; Shen, B.G.; Gao, B.; Shen, J.; Sun, J.R. The magnetocaloric effect of $\text{LaFe}_{11.6}\text{Si}_{1.4}$, $\text{La}_{0.8}\text{Nd}_{0.2}\text{Fe}_{11.5}\text{Si}_{1.5}$, and $\text{Ni}_{43}\text{Mn}_{46}\text{Sn}_{11}$ compounds in the vicinity of the first-order phase transition. *Adv. Mater.* **2009**, *21*, 693–696. [[CrossRef](#)]
16. Shen, B.G.; Sun, J.R.; Hu, F.X.; Zhang, H.W.; Cheng, Z.H. Recent Progress in Exploring Magnetocaloric Materials. *Adv. Mater.* **2009**, *21*, 4545–4564. [[CrossRef](#)]
17. Lyubina, J.; Schafer, R.; Martin, N.; Schultz, L.; Gutfleisch, O. Novel design of $\text{La}(\text{Fe},\text{Si})_{13}$ alloys towards high magnetic refrigeration performance. *Adv. Mater.* **2010**, *22*, 3735–3739. [[CrossRef](#)] [[PubMed](#)]
18. Hu, F.X.; Shen, B.G.; Sun, J.R.; Zhang, X.X. Great magnetic entropy change in $\text{La}(\text{Fe},\text{M})_{13}$ (M=Si, Al) with Co doping. *Chin. Phys.* **2000**, *9*, 550–556.
19. Gutfleisch, O.; Yan, A.; Müller, K.H. Large magnetocaloric effect in melt-spun $\text{LaFe}_{13-x}\text{Si}_x$. *J. Appl. Phys.* **2005**, *97*, 10M305. [[CrossRef](#)]
20. Zhong, X.C.; Feng, X.L.; Huang, J.H.; Zhang, H.; Huang, Y.L.; Liu, Z.W.; Jiao, D.L. Microstructure evolution and large magnetocaloric effect of $\text{La}_{0.8}\text{Ce}_{0.2}(\text{Fe}_{0.95}\text{Co}_{0.05})_{11.8}\text{Si}_{1.2}$ alloy prepared by strip-casting and annealing. *Aip Adv.* **2018**, *8*, 048102.
21. Liu, X.B.; Altounian, Z. Effect of Co content on magnetic entropy change and structure of $\text{La}(\text{Fe}_{1-x}\text{Co}_x)_{11.4}\text{Si}_{1.6}$. *J. Magn. Magn. Mater.* **2003**, *264*, 209–213. [[CrossRef](#)]
22. Hu, F.X.; Gao, J.; Qian, X.L.; Ilyn, M.; Tishin, A.M.; Sun, J.R.; Shen, B.G. Magnetocaloric effect in itinerant electron metamagnetic systems $\text{La}(\text{Fe}_{1-x}\text{Co}_x)_{11.9}\text{Si}_{1.1}$. *J. Appl. Phys.* **2005**, *97*, 10M303. [[CrossRef](#)]
23. Fujita, A.; Fujieda, S.; Hasegawa, Y.; Fukamichi, K. Itinerant-electron metamagnetic transition and large magnetocaloric effects in $\text{La}(\text{Fe}_x\text{Si}_{1-x})_{13}$ compounds and their hydrides. *Phys. Rev.* **2003**, *B67*, 104416. [[CrossRef](#)]
24. Fujieda, S.; Fujita, A.; Fukamichi, K. Enhancements of magnetocaloric effects in $\text{La}(\text{Fe}_{0.90}\text{Si}_{0.10})_{13}$ and its hydride by partial substitution of Ce for La. *Mater. Trans.* **2004**, *45*, 3228–3231. [[CrossRef](#)]
25. Mandal, K.; Pal, D.; Gutfleisch, O.; Kersch, P.; Müller, K.H. Magnetocaloric effect in reactively-milled $\text{LaFe}_{11.57}\text{Si}_{1.43}\text{H}_y$ intermetallic compounds. *J. Appl. Phys.* **2007**, *102*, 053906. [[CrossRef](#)]
26. Krautz, M.; Moore, J.D.; Skokov, K.P.; Liu, J.; Teixeira, C.S.; Schäfer, R.; Schultz, L.; Gutfleisch, O. Reversible solid-state hydrogen-pump driven by magnetostructural transformation in the prototype system $\text{La}(\text{Fe},\text{Si})_{13}\text{H}_y$. *J. Appl. Phys.* **2012**, *112*, 083918. [[CrossRef](#)]
27. Lyubina, J.; Hannemann, U.; Ryan, M.P.; Cohen, L.F. Electrolytic hydriding of $\text{LaFe}_{13-x}\text{Si}_x$ alloys for energy efficient magnetic cooling. *Adv. Mater.* **2012**, *24*, 2042–2046. [[CrossRef](#)] [[PubMed](#)]
28. Zheng, H.; Tang, Y.; Chen, Y.; Wu, J.; Wang, H.; Xue, X.; Wang, J.; Pang, W. The high-temperature hydrogenation behavior of $\text{LaFe}_{11.6}\text{Si}_{1.4}$ and splitting of $\text{LaFe}_{11.6}\text{Si}_{1.4}\text{H}_y$ magnetocaloric transition. *J. Alloys Compd.* **2015**, *646*, 124–128. [[CrossRef](#)]
29. Hu, F.X.; Chen, L.; Wang, J.; Bao, L.F.; Sun, J.R.; Shen, B.G. Particle size dependent hysteresis loss in $\text{La}_{0.7}\text{Ce}_{0.3}\text{Fe}_{11.6}\text{Si}_{1.4}\text{Co}_{0.2}$ first-order systems. *Appl. Phys. Lett.* **2012**, *100*, 072403. [[CrossRef](#)]
30. Skokov, K.; Karpenkov, D.; Kuz'Min, M.D.; Radulov, I.A.; Gottschall, T.; Kaeswurm, B.; Fries, M.; Gutfleisch, O. Heat exchangers made of polymer-bonded $\text{La}(\text{Fe},\text{Si})_{13}$. *J. Appl. Phys.* **2014**, *115*, 17A941. [[CrossRef](#)]
31. Liu, J.; Zhang, M.X.; Shao, Y.Y.; Yan, A.R. $\text{LaFe}_{11.6}\text{Si}_{1.4}/\text{Cu}$ magnetocaloric composites prepared by hot pressing. *IEEE Trans. Magn.* **2015**, *51*, 2501502.
32. Zhang, H.; Liu, J.; Zhang, M.; Shao, Y.; Li, Y.; Yan, A. $\text{LaFe}_{11.6}\text{Si}_{1.4}\text{H}_y/\text{Sn}$ magnetocaloric composites by hot pressing. *Scr. Mater.* **2016**, *120*, 58–61. [[CrossRef](#)]
33. Dong, X.T.; Zhong, X.C.; Peng, D.R.; Huang, J.H.; Zhang, H.; Jiao, D.L.; Liu, Z.W.; Ramanujan, R.V. $\text{La}_{0.8}\text{Ce}_{0.2}(\text{Fe}_{0.95}\text{Co}_{0.05})_{11.8}\text{Si}_{1.2}/\text{Sn}_{42}\text{Bi}_{58}$ magnetocaloric composites prepared by low temperature hot pressing. *J. Alloys Compd.* **2018**, *737*, 568–574. [[CrossRef](#)]

34. Zhong, X.C.; Peng, D.R.; Dong, X.T.; Huang, J.H.; Zhang, H.; Jiao, D.L.; Liu, Z.W.; Ramanujan, R.V. Improvement in the magnetocaloric properties of sintered La(Fe,Si)₁₃ based composites processed by La-Co grain boundary diffusion. *J. Alloys Compd.* **2019**, *780*, 873–880. [[CrossRef](#)]
35. Zhong, X.C.; Peng, D.R.; Dong, X.T.; Huang, J.H.; Zhang, H.; Huang, Y.L.; Wu, S.M.; Yu, H.Y.; Qiu, W.Q.; Liu, Z.W.; et al. Improvement in mechanical and magnetocaloric properties of hot-pressed La(Fe,Si)₁₃/La₇₀Co₃₀ composites by grain boundary engineering. *Mater. Sci. Eng. B* **2021**, *263*, 114900. [[CrossRef](#)]
36. Zhang, R.F.; Zhang, S.H.; He, Z.J.; Jing, J.; Sheng, S.H. Miedema Calculator: A thermodynamic platform for predicting formation enthalpies of alloys within framework of Miedema's Theory. *Comput. Phys. Commun.* **2016**, *209*, 58–69. [[CrossRef](#)]
37. Guo, Q.W.; Wang, G.S.; Guo, G.C. *Non-Ferrous Metal Atlas of Binary Alloy Phase*; Chemical Industry Press: Beijing, China, 2010.
38. Zhou, Q.; Liu, Z.W.; Zhong, X.C.; Zhang, G.Q. Properties improvement and structural optimization of sintered NdFeB magnets by non-rare earth compound grain boundary diffusion. *Mater. Des.* **2015**, *86*, 114–120. [[CrossRef](#)]
39. Chen, X.; Chen, Y.G.; Tang, Y.B. The effect of high-temperature annealing on LaFe_{11.5}Si_{1.5} and the magnetocaloric properties of La_{1-x}Ce_xFe_{11.5}Si_{1.5} compounds. *Rare Metals* **2011**, *30*, 343–347. [[CrossRef](#)]
40. Fan, W.B.; Hou, Y.H.; Ge, X.J.; Huang, Y.L.; Luo, J.M.; Zhong, Z.C. Microstructure and improved magnetocaloric properties: LaFeSi/LaAl magnets prepared by spark plasma sintering technique. *J. Phys. D Appl. Phys.* **2018**, *51*, 115003. [[CrossRef](#)]
41. Zhong, X.C.; Dong, X.T.; Peng, D.R.; Huang, J.H.; Zhang, H.; Jiao, D.L.; Zhang, H.; Liu, Z.W.; Ramanujan, R.V. Table-like magnetocaloric effect and enhanced refrigerant capacity of HPS La(Fe,Si)₁₃ based composites by Ce-Co grain boundary diffusion. *J. Mater. Sci.* **2020**, *55*, 5908–5919. [[CrossRef](#)]
42. Löwe, K.; Liu, J.; Skokov, K.; Moore, J.D.; Amin, H.S.; Hono, K.; Katter, M.; Gutfleisch, O. The effect of the thermal decomposition reaction on the mechanical and magnetocaloric properties of La(Fe,Si,Co)₁₃. *Acta Mater.* **2012**, *60*, 4268–4276. [[CrossRef](#)]
43. Liu, J.; Krautz, M.; Skokov, K.; Woodcock, T.G.; Gutfleisch, O. Systematic study of the microstructure, entropy change and adiabatic temperature change in optimized La-Fe-Si alloys. *Acta Mater.* **2011**, *59*, 3602–3611. [[CrossRef](#)]
44. Predel, B. Ce-Co (Cerium-Cobalt) phase diagram. In *Phase Equilibria, Crystallographic and Thermodynamic Data of Binary Alloys Landolt-Börnstein: Numerical Data and Functional Relationships in Science and Technology-New Series*; Springer: Berlin/Heidelberg, Germany, 1993; Volume 3, ISBN 9783540614333.
45. Laptev, A.V. Structure and properties of WC-Co alloys in solid-phase sintering. I. Geometrical evolution. *Powder Met. Met. Ceram.* **2007**, *46*, 415–422. [[CrossRef](#)]
46. Pribytkov, G.A.; Andreeva, I.A.; Korzhova, V.V. Bulk changes and structure formation in solid-phase sintering of Ti – TiAl₃ powder mixtures. *Powder Met. Met. Ceram.* **2008**, *47*, 687–692. [[CrossRef](#)]
47. Itoh, M.; Machida, K.I.; Hirose, K.; Adachi, G.Y. Nitrogen absorption and desorption characteristics for CeFe₇. *Chem. Lett.* **2001**, *30*, 294–295. [[CrossRef](#)]
48. Hou, X.L.; Lampen-Kelley, P.; Xue, Y.; Liu, C.Y.; Xu, H.; Han, N.; Ma, C.W.; Srikanth, H.; Phan, M.H. Formation mechanisms of NaZn₁₃-type phase in giant magnetocaloric La-Fe-Si compounds during rapid solidification and annealing. *J. Alloys Compd.* **2015**, *646*, 503–511. [[CrossRef](#)]
49. Krypiakewytsch, P.I.; Zaretschniuk, O.S.; Hladyschewskyj, E.I. Ternäre verbindungen vom NaZn₁₃-type. *Z. Anorg. Allg. Chem.* **1968**, *358*, 90–96. [[CrossRef](#)]
50. Passamani, E.C.; Larica, C.; Proveti, J.R.; Takeuchi, A.Y.; Gomes, A.M.; Ghivelder, L. Magnetic and magnetocaloric properties of La(Fe,Co)_{11.4}SP_{1.6} compounds (SP=Al or Si). *J. Magn. Magn. Mater.* **2007**, *312*, 65–71. [[CrossRef](#)]
51. Shao, Y.Y.; Liu, Y.F.; Wang, K.; Zhang, M.X.; Liu, J. Impact of interface structure on functionality in hot-pressed La-Fe-Si/Fe magnetocaloric composites. *Acta Mater.* **2020**, *195*, 163–171. [[CrossRef](#)]
52. Zhang, M.X.; Ouyang, Y.; Zhang, Y.F.; Liu, J. LaFe₁₁Co_{0.8}Si_{1.2}/Al magnetocaloric composites prepared by hot pressing. *J. Alloys Compd.* **2020**, *823*, 153846. [[CrossRef](#)]
53. Wang, Y.X.; Zhang, H.; Liu, E.K.; Zhong, X.C.; Tao, K.; Wu, M.L.; Xing, C.F.; Xiao, Y.N.; Liu, J.; Long, Y. Outstanding comprehensive performance of La(Fe,Si)₁₃H_y/In composite with durable service life for magnetic refrigeration. *Adv. Electron. Mater.* **2018**, *4*, 1700636. [[CrossRef](#)]
54. Gschneidner, K.A., Jr.; Pecharsky, V.K. Magnetocaloric materials. *Annu. Rev. Mater. Sci.* **2000**, *30*, 387–429. [[CrossRef](#)]
55. Fujieda, S.; Fukamichi, K.; Suzuki, S. Microstructure and isothermal magnetic entropy change of La(Fe_{0.89}Si_{0.11})₁₃ in a single-phase formation process by annealing. *J. Alloys Compd.* **2013**, *566*, 196–200. [[CrossRef](#)]
56. Wu, S.M.; Zhong, X.C.; Dong, X.T.; Liu, C.L.; Huang, J.H.; Huang, Y.L.; Yu, H.Y.; Liu, Z.W.; Huang, Y.S.; Ramanujan, R.V. LaFe_{11.6}Si_{1.4}/Pr₄₀Co₆₀ magnetocaloric composites for refrigeration near room temperature. *J. Alloys Compd.* **2021**, *873*, 159796. [[CrossRef](#)]
57. Yu, P.; Zhang, N.Z.; Cui, Y.T.; Wu, Z.M.; Wen, L.; Zeng, Z.Y.; Xia, L. Achieving better magneto-caloric effect near room temperature in amorphous Gd₅₀Co₅₀ alloy by minor Zn addition. *J. Non-Crystall. Solids* **2016**, *434*, 36–40. [[CrossRef](#)]
58. Dan'Kov, S.Y.; Tishin, A.M.; Pecharsky, V.K.; Gschneidner, K.A., Jr. Magnetic phase transitions and the magnetothermal properties of gadolinium. *Phys. Rev. B* **1998**, *57*, 3478–3490. [[CrossRef](#)]
59. Zhong, X.C.; Tian, H.C.; Wang, S.S.; Liu, Z.W.; Zheng, Z.G.; Zeng, D.C. Thermal, magnetic and magnetocaloric properties of Fe_{80-x}M_xB₁₀Zr₉Cu₁ (M = Ni, Ta; x = 0, 3, 5) amorphous alloys. *J. Alloys Compd.* **2015**, *633*, 188–193. [[CrossRef](#)]

-
60. Banerjee, B.K. On a generalised approach to first and second order magnetic transitions. *Phys. Lett.* **1964**, *12*, 16–17. [[CrossRef](#)]
 61. Hu, F.X. *Magnetic and Magnetic Entropy Changes of Fe-Based La(Fe,M)₁₃ Compounds and Ni-Mn-Ga Alloys*; Institute of Physics, Chinese Academy of Sciences: Beijing, China, 2002. (In Chinese)